Electronic Supplementary Material (ESI) for Journal of Materials Chemistry A.

— Electronic Supplementary Information —

Doping by Design: Finding New n-type ABX_4 Zintl Phases for Thermoelectrics

Jiaxing Qu,[†] Vladan Stevanović,[‡] Elif Ertekin,[†] and Prashun Gorai[*,‡]

[†]*University of Illinois at Urbana-Champaign, Urbana, IL 61801*

[‡]*Colorado School of Mines, Golden, CO 80401*

E-mail: pgorai@mines.edu

1. Fitted Elemental-Phase Reference Chemical Potentials

The fitted elemental-phase reference energies used in calculating the phase stability region (μ_i^0 in **Eq. 2**): Li: -1.74 eV, Na: -1.24 eV, K: -1.14 eV, Rb: -0.82 eV, Cs: -0.96 eV, Al: -3.55 eV, Ga: -3.12 eV, In: -2.62 eV, As: -4.59 eV, Sb: -4.11 eV, Bi: -4.19 eV

2. ABX_4 Structures from ICSD Considered for Assessing Structural Stability

$RbAlF_4$ (123), $KAlF_4$ (123), $CuGaCl_4$ (112), $CuGaI_4$ (82), $CuAuSe_4$ (11), $CuAlCl_4$ (112), $CuAlBr_4$ (112), $AgAuTe_4$ (13), $RbFeF_4$ (127), $NaMnF_4$ (14), $CsCrF_4$ (189), $RbFeF_4$ (18), $KAlF_4$ (11), $KFeF_4$ (63), $RbMnF_4$ (14), $RbFeF_4$ (57), $CsFeF_4$ (129), $TlAlF_4$ (15), $TlAlF_4$ (140), $LiMnO_4$ (63), $NaTiF_4$ (60), $KAuI_4$ (14), $KAuCl_4$ (14), $RbAlF_4$ (59), $LiAuF_4$ (13), $LiAuF_4$ (15), $CsAuF_4$ (71), $CsMnF_4$ (85), $AlInI_4$ (11), $TlMnF_4$ (15), $KTlF_4$ (144), $KScF_4$ (12), $KFeF_4$ (31), $CsReBr_4$ (61).

Numbers in parentheses denote the space group number.

3. Γ-point Frequencies of Phonon Modes

Table S1: Γ-point phonon frequencies of the 13 Zintl phases predicted to be stable in the $KGaSb_4$ structure type, given in THz. Only the 10 lowest frequency modes are shown, including the three acoustic modes.

	Phonon mode index									
Compound	1	2	3	4	5	6	7	8	9	10
$NaGaSb_4$	0.00	0.00	0.00	0.98	1.03	1.12	1.15	1.17	1.41	1.42
$NaAlSb_4$	0.00	0.00	0.00	0.61	0.66	0.68	0.79	0.80	0.93	0.93
$CsInSb_4$	-0.03	-0.02	0.00	0.54	0.57	0.58	0.59	0.65	0.70	0.87
$CsGaSb_4$	-0.01	0.00	0.00	0.60	0.70	0.72	0.76	0.78	0.79	0.97
$RbInSb_4$	0.00	0.00	0.00	0.55	0.57	0.59	0.64	0.68	0.69	0.90
$KInSb_4$	0.00	0.00	0.00	0.54	0.62	0.62	0.68	0.69	0.71	0.91
$CsAlSb_4$	-0.03	-0.01	0.01	0.61	0.65	0.67	0.73	0.79	0.79	0.94
$RbGaSb_4$	0.00	0.00	0.00	0.63	0.67	0.70	0.78	0.78	0.84	1.03
$KGaSb_4$	0.00	0.00	0.00	0.66	0.69	0.69	0.78	0.82	0.89	1.08
$RbAlSb_4$	0.00	0.00	0.00	0.65	0.67	0.68	0.77	0.78	0.84	1.04
$KGaAs_4$	0.00	0.00	0.00	0.98	1.03	1.07	1.09	1.24	1.30	1.58
$KAlSb_4$	0.00	0.00	0.00	0.64	0.71	0.71	0.78	0.81	0.89	1.09
$NaGaAs_4$	0.00	0.00	0.00	0.62	0.67	0.68	0.71	0.82	0.87	0.88

4. Electronic Structures of Stable ABX_4 Zintl Phases

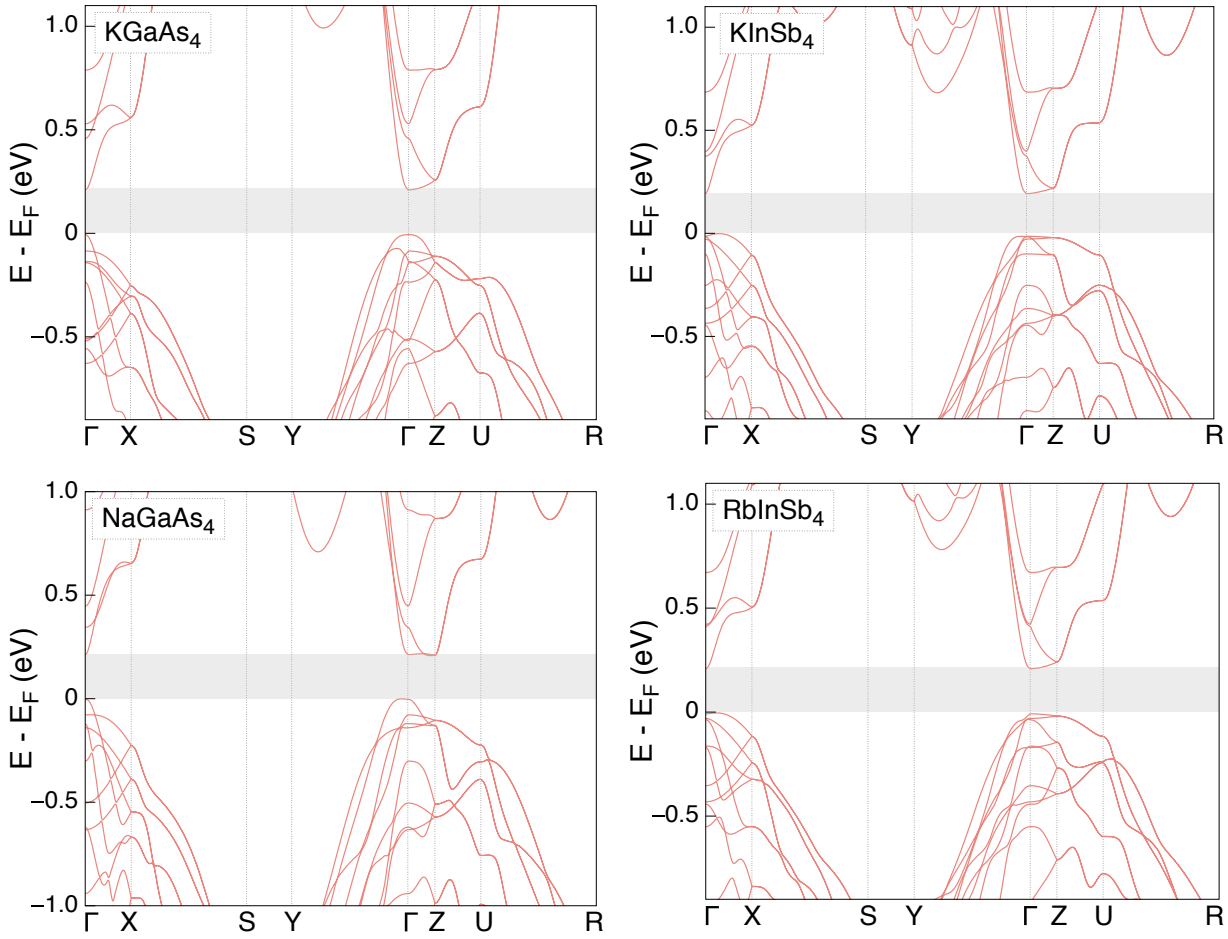

Figure S1: Electronic structures (GGA-PBE) of $KGaAs_4$, $KInSb_4$, $NaGaAs_4$, and $RbInSb_4$ along the special k-point paths of the Brillouin zone.

5. Electronic Structure of $CsInSb_4$ with Spin-Orbit Coupling

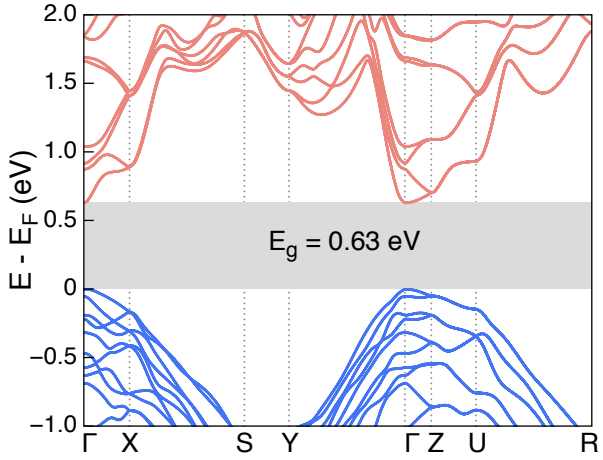

Figure S2: Electronic structure of $CsInSb_4$ along the special k-point paths of the Brillouin zone. Note that the band edge positions are obtained from GW quasi-particle energy calculations and spin-orbit coupling (at the DFT level of theory).

6. Predicted Thermoelectric Performance

Table S2: Computed electronic structure and transport parameters, and thermoelectric performance of 13 ABX_4 Zintl phases that are predicted to be stable in the $KGaSb_4$ structure. β is referenced to β of PbTe (15 for both p- and n-type). β_p and β_n are p- and n-type thermoelectric quality factor, E_g is DFT band gap, B is bulk modulus, $m^*_{\mathrm{DOS,VB}}$ and $m^*_{\mathrm{DOS,CB}}$ are density-of-states effective masses of valence and conduction bands, $N_{\mathrm{b,VB}}$ and $N_{\mathrm{b,CB}}$ are valence and conduction band degeneracies, μ_p and μ_n are room-temperature hole and electron mobilities, and κ_L is room-temperature lattice thermal conductivity.

Phases	$\beta_p/\beta_{\mathrm{PbTe}}$	$\beta_n/\beta_{\mathrm{PbTe}}$	E_g (eV)	B (GPa)	$m^*_{\mathrm{DOS,VB}}$ (m_e)	$m^*_{\mathrm{DOS,CB}}$ (m_e)	$N_{\mathrm{b,VB}}$	$N_{\mathrm{b,CB}}$	μ_p (cm^2/Vs)	μ_n (cm^2/Vs)	κ_{L} (W/mK)
$NaGaSb_4$	0.7	4.8	0.19	19.9	0.43	0.33	2	7	17	88	1.0
$NaAlSb_4$	0.7	4.5	0.12	19.8	0.43	0.24	2	6	17	124	1.0
$CsInSb_4$	1.0	1.7	0.25	29.0	1.59	0.14	4	2	7	136	1.2
$CsGaSb_4$	0.5	1.7	0.30	18.9	0.80	0.11	2	2	6	117	0.9
$RbInSb_4$	1.1	1.6	0.22	28.8	1.29	0.13	4	2	9	141	1.2
$KInSb_4$	1.5	1.6	0.19	30.3	1.32	0.13	5	2	12	150	1.3
$CsAlSb_4$	0.8	1.5	0.32	19.3	1.00	0.59	3	2	7	98	0.9
$RbGaSb_4$	1.1	1.5	0.30	19.0	0.51	0.12	3	2	19	105	0.9
$KGaSb_4$	0.3	1.5	0.25	19.2	0.30	0.12	1	2	14	106	1.0
$RbAlSb_4$	0.3	1.4	0.26	19.3	0.34	0.14	1	2	12	88	1.0
$KGaAs_4$	0.8	1.4	0.22	26.9	0.85	0.14	3	2	12	123	1.4
$KAlSb_4$	0.3	1.3	0.21	19.6	0.26	0.14	1	2	18	93	1.0
$NaGaAs_4$	0.5	1.2	0.21	28.2	0.71	0.18	2	2	11	93	1.4

7. Defect Chemistry of ABX_4 Zintl Phases Under Alkali-Poor Conditions

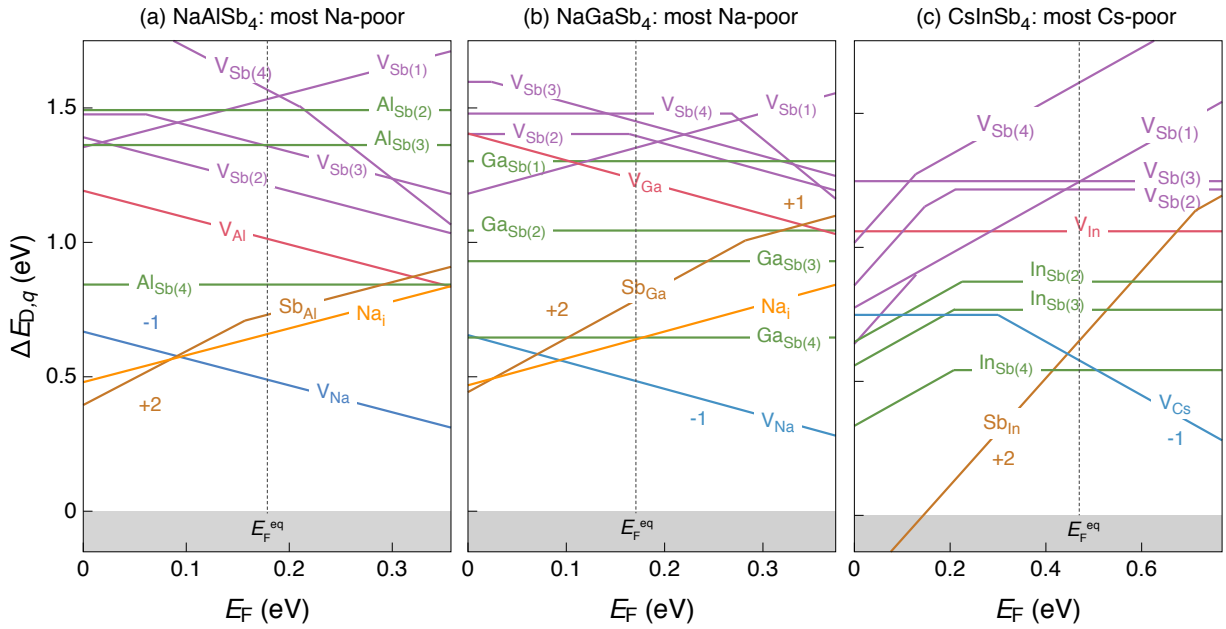

Figure S3: Formation energies of native defects ($\Delta E_{\mathrm{D},q}$) as a function of Fermi energy (E_{F}) for (a) $NaAlSb_4$ (under the most Na-poor conditions), (b) $NaGaSb_4$ (under the most Na-poor condition), (c) $CsInSb_4$ (under the most Cs-poor condition). E_{F} is referenced to the valence band maximum and E_{F} values can range from 0 to the band gap. The slope of the line is equal to the charge state of the defect. The lowest energy acceptors are alkali vacancies (in blue). The equilibrium E_{F} (dashed vertical lines) is calculated at 800 K.

8. Optimized Crystal Structures of 7 New ABX_4 Zintl Phases

VASP POSCAR files available at:

github.com/prashungorai/papers/tree/main/2020/abx4zintls